Chapter 4
Spectral Correlation Function for the Electromagnetic Field from Planar Sources

The spectral correlation function for the fluctuating electromagnetic field outside a semi-infinite solid with a planar surface can be calculated using the generalized Kirchhoff law for isotropic materials. For the more general case of anisotropic materials, the same quantity is calculated using the Green function approach. The local density of state of the electromagnetic field is calculated and analyzed in the near-field. In the near-field, the thermal electromagnetic field can be spatially and temporally coherent due to the existence of the surface plasmons or surface phonon polaritons. We show that due to the coupling of the evanescent and propagating electromagnetic waves introduced by a grating, the coherent properties of the electromagnetic field in the near-field can be used to design highly directional (as compared with Lambertian emission) thermal sources working in the far-field.

4.1 Generalized Kirchhoff Law

The theory presented in Sect. 3.2 can be used to calculate the spectral correlation functions for an electromagnetic field radiated by any body. A particularly important limiting case is the radiation from a flat surface. In Appendix A, these correlation functions are calculated using the general theory of a fluctuating electromagnetic field. However, for the planar geometry, these correlation functions can be obtained in a simpler way using the generalized Kirchhoff law. According to the classical Kirchhoff low, the intensity of emission of radiation from a flat element of a body surface in certain direction at a fixed frequency is given by

$$I(\omega, \theta, \phi) = I_0(\omega)[1 - \kappa(\omega, \theta, \phi)] \tag{4.1}$$

where θ is the angle between the normal to the surface and the direction to the radiation detector, ϕ is the azimuthal angle in plane of the sample surface, $\kappa(\omega, \theta, \phi)$ is the energy reflection coefficient of the body at a given frequency of the field in the direction specified by the polar and azimuthal angles θ and ϕ, and $I_0(\omega)$ is the

A.I. Volokitin and B.N.J. Persson, *Electromagnetic Fluctuations at the Nanoscale*,
NanoScience and Technology, DOI 10.1007/978-3-662-53474-8_4

equilibrium intensity of emission, which for a closed cavity is independent of the incidence angle and of the material. In cases of isotropic materials, $\kappa(\omega, \theta, \phi) = \kappa(\omega, \theta)$.

For planar geometry, the electromagnetic field can be decomposed on s- and p-polarized electromagnetic fields. In this representation, the electric field of the emitted radiation can be written in the form

$$\mathbf{E}(\mathbf{r}, \omega) = \int \frac{d^2q}{(2\pi)^2} \left[E_s(q, \omega)\hat{n} + E_p(q, \omega)\hat{\mathbf{K}} \right] e^{i(\mathbf{q}\cdot\mathbf{x} + k_z z)} \tag{4.2}$$

where $\mathbf{r} = (\mathbf{x}, z), k_z = \sqrt{(\omega/c)^2 - q^2}, \hat{q} = \mathbf{q}/q,\ \hat{n} = \hat{z}\times\hat{q}, \hat{\mathbf{K}} = (q\hat{z} - k_z\hat{q})/k,\ k = \omega/c$. The spectral spatial correlation function can be written in the form

$$\left\langle \mathbf{E}(\mathbf{r})\mathbf{E}^*(\mathbf{r}') \right\rangle_\omega = \int \frac{d^2q}{(2\pi)^2} \left[\hat{n} w_s \hat{n} + \hat{\mathbf{K}} w_p \hat{\mathbf{K}}^* \right] e^{i\mathbf{q}\cdot(\mathbf{x}-\mathbf{x}')} e^{i(k_z z - k_z^* z')}, \tag{4.3}$$

where $w_s = \left\langle |E_s(q, \omega)|^2 \right\rangle$ and $w_p = \left\langle |E_p(q, \omega)|^2 \right\rangle$.

The Kirchhoff law is the consequence of the energy conservation law: the intensity of the emitted radiation in thermal equilibrium should be equal to the absorbed energy. Therefore, the Kirchhoff law can be written separately for the s- and p-components of the electromagnetic field. Taking into account that the intensity of the electromagnetic wave is proportional to $\langle |E_{s(p)}|^2 \rangle$, the Kirchhoff law can be written in the form

$$\langle |E_{s(p)}(q, \omega)|^2 \rangle = \langle |E_{0,s(p)}(q, \omega)|^2 \rangle \left[1 - |R_{s(p)}(q, \omega)| \right] \tag{4.4}$$

where $E_{0,s(p)}(q, \omega)$ is the amplitude of the incident plane wave of black body radiation, and where $R_{p(s)}$ is the reflection amplitude for $p(s)$-polarized electromagnetic field. Taking into account that the energy density of the plane wave in the black body radiation can be written in the form (see (3.54) and (3.61)):

$$\begin{aligned} &\frac{1}{8\pi} \left[\langle 2|E_{s(p)}(q, \omega)|^2 \rangle + 2\langle |B_{s(p)}(q, \omega)|^2 \rangle \right] \frac{d^2q}{(2\pi)^2} d\omega \\ &\quad = \frac{1}{2\pi} \langle |E_{s(p)}(q, \omega)|^2 \rangle \frac{d^2q}{(2\pi)^2} d\omega \\ &\quad = \hbar\omega \left(\frac{1}{2} + \frac{1}{e^{(\hbar\omega/k_B T)} - 1} \right) \frac{d^2q}{(2\pi)^2} \frac{dk_z}{2\pi} = \frac{\hbar k^2}{4\pi k_z} \coth\left(\frac{\hbar\omega}{2k_B T} \right) \frac{d^2q}{(2\pi)^2} d\omega \end{aligned} \tag{4.5}$$

for the propagating electromagnetic waves we get

$$w_{p(s)}^{prop} = \coth\left(\frac{\hbar\omega}{2k_B T} \right) \frac{\hbar k^2}{2k_z} \left(1 - |R_{ps}|^2 \right) \tag{4.6}$$

To calculate the spectral correlation function for evanescent waves, we will assume that above the surface of the body at the point $\mathbf{r} = \mathbf{r}'$ there is a small particle with

fluctuating dipole moment $\mathbf{p}^f$, which is characterized by the spectral function of fluctuations

$$\left\langle p_i^f \, p_j^f \right\rangle_\omega = \frac{\hbar}{\pi}\left(\frac{1}{2} + n_i(\omega)\right) \mathrm{Im}\alpha(\omega)\delta_{ij}, \tag{4.7}$$

where $\alpha(\omega)$ is the polarizability of the particle. At each $\mathbf{q}$ it is convenient to choose coordinate axes along vectors $\hat{q}$, $\hat{n}$, $\hat{z}$. The energy absorbed by the particle due to interaction with the electromagnetic field emitted by the body is given by

$$\dot{Q}_s^{part}(q,\omega) = \mathrm{Re}(-i\omega\mathbf{p}^{ind}\cdot\mathbf{E}_s^*) = \omega\mathrm{Im}\alpha(\omega)|E_s|^2 e^{-2\mathrm{Im}k_z z'} \tag{4.8}$$

$$\dot{Q}_p^{part}(q,\omega) = \mathrm{Re}(-i\omega\mathbf{p}^{ind}\cdot\mathbf{E}_p^*) = \omega\mathrm{Im}\alpha(\omega)|E_p|^2\frac{q^2+|k_z|^2}{k^2}e^{-2\mathrm{Im}k_z z'} \tag{4.9}$$

where $\mathbf{p}^{ind} = \alpha(\omega)\mathbf{E}$ is the induced dipole moment of the particle. The electromagnetic field at the point $\mathbf{r}$ created by the particle located at the point $\mathbf{r}'$ (assuming $z < z'$) can be written in the form

$$\mathbf{E}_s^{part}(\mathbf{r},\mathbf{r}') = \frac{2\pi i k^2}{k_z}\left(e^{ik_z(z'-z)} + R_s e^{ik_z(z+z')}\right) p_n^f \hat{n} e^{i\mathbf{q}\cdot(\mathbf{x}-\mathbf{x}')}, \tag{4.10}$$

$$\begin{aligned}\mathbf{E}_p^{part} = \frac{2\pi i}{k_z}\Big[&\left(e^{ik_z(z'-z)} + R_p e^{ik_z(z+z')}\right) q\hat{z} \\ &+ \left(e^{ik_z(z'-z)} - R_p e^{ik_z(z+z')}\right) k_z\hat{q}\Big](k_z p_q^f + q f_z^f) e^{i\mathbf{q}\cdot(\mathbf{x}-\mathbf{x}')},\end{aligned} \tag{4.11}$$

$$\mathbf{B}_s^{part} = \frac{2\pi i k}{k_z}\left[\left(e^{ik_z(z'-z)} + R_s e^{ik_z(z+z')}\right) q\hat{z} + \left(e^{ik_z(z'-z)} - R_s e^{ik_z(z+z')}\right) k_z\hat{q}\right] p_n^f e^{i\mathbf{q}\cdot(\mathbf{x}-\mathbf{x}')}, \tag{4.12}$$

$$\mathbf{B}_p^{part}(\mathbf{r},\mathbf{r}') = -\frac{2\pi i k}{k_z}\left(e^{ik_z(z'-z)} + R_p e^{ik_z(z+z')}\right)(k_z p_q^f + q f_z^f)\hat{n} e^{i\mathbf{q}\cdot(\mathbf{x}-\mathbf{x}')}. \tag{4.13}$$

The energy absorbed by the body due to interaction with the evanescent waves created by the particle is determined by the z-component of the Poynting vector and can be written separately for p- and s-polarized waves:

$$\begin{aligned}\dot{Q}_s^b =& \frac{c}{8\pi}\left(\langle E_n B_q^*\rangle + c\cdot c\right) = \coth\left(\frac{\hbar\omega}{2k_B T}\right)\frac{\hbar c k^3}{4|k_z|^2} \\ &\times (k_z - k_z^*)(R_s^* - R_s)\mathrm{Im}\alpha(\omega)e^{-2\mathrm{Im}k_z z'},\end{aligned} \tag{4.14}$$

$$\dot{Q}_p^b = \frac{c}{8\pi}\left(\langle E_q B_n^*\rangle + c\cdot c\right) = \coth\left(\frac{\hbar\omega}{2k_BT}\right)\frac{\hbar ck^3}{4|k_z|^2} \times (k_z - k_z^*)(R_p^* - R_p)\mathrm{Im}\alpha(\omega)\frac{q^2+|k_z|^2}{k^2}e^{-2\mathrm{Im}k_z z'}. \tag{4.15}$$

In the thermal equilibrium, the energy absorbed by the particle should be equal to the energy absorbed by the body. From this condition, and using (4.8), (4.9), (4.14) and (4.15) we get

$$w_{s(p)}^{evan} = \coth\left(\frac{\hbar\omega}{2k_BT}\right)\frac{\hbar k^2}{4|k_z|^2}\left(k_z - k_z^*\right)\left(R_{s(p)}^* - R_{s(p)}\right) \tag{4.16}$$

Taking into account that k_z is pure real for the propagating waves ($q < k$) and pure imaginary for the evanescent waves ($q > k$), the contribution to $w_{p(s)}$ from propagating waves can be written in the form

$$w_{p(s)}^{prop} = \coth\left(\frac{\hbar\omega}{2k_BT}\right)\frac{\hbar k^2}{4|k_z|^2}\left(k_z + k_z^*\right)\left(1 - |R_{ps}|^2\right) \tag{4.17}$$

Summarizing (4.16) and (4.17) we finally get

$$w_{s(p)} = w_{s(p)}^{prop} + w_{s(p)}^{evan} = \coth\left(\frac{\hbar\omega}{2k_BT}\right)\frac{\hbar k^2}{4|k_z|^2} \times \left[(k_z + k_z^*)(1 - |R_{p(s)}|^2) + (k_z - k_z^*)(R_{s(p)}^* - R_{s(p)})\right] \tag{4.18}$$

Using Maxwell's equation

$$\nabla \times \mathbf{E}(\mathbf{r}) = \frac{i\omega}{c}\mathbf{B}(\mathbf{r}),$$

from (4.3), we get the spectral correlation function for the magnetic induction field

$$\left\langle \mathbf{B}(\mathbf{r})\mathbf{B}(\mathbf{r}')\right\rangle_\omega = \coth\left(\frac{\hbar\omega}{2k_BT}\right)\int\frac{d^2q}{(2\pi)^2}\left[\hat{n}w_p\hat{n} + \hat{\mathbf{K}}w_s\hat{\mathbf{K}}^*\right]e^{i\mathbf{q}\cdot(\mathbf{x}-\mathbf{x}')}e^{i(k_z z - k_z^* z')}, \tag{4.19}$$

and the spectral cross-correlation function

$$\left\langle \mathbf{E}(\mathbf{r})\mathbf{B}(\mathbf{r}')\right\rangle_\omega = \coth\left(\frac{\hbar\omega}{2k_BT}\right)\int\frac{d^2q}{(2\pi)^2}\left[\hat{\mathbf{K}}w_p\hat{n} + \hat{n}w_s\hat{\mathbf{K}}^*\right]e^{i\mathbf{q}\cdot(\mathbf{x}-\mathbf{x}')}e^{i(k_z z - k_z^* z')}. \tag{4.20}$$

Using (4.20), we can calculate the intensity of the radiated energy $I(\omega)$ into vacuum at $T = 0$ K:

$$I(\omega)d\omega = 2\left[\langle S_z(T,\omega)\rangle - \langle S_z(0,\omega)\rangle\right]d\omega, \tag{4.21}$$

where the factor 2 arises for the same reason as in (3.54). The z-component of the Poynting vector is given by

$$\begin{aligned}\langle S_z(T,\omega)\rangle &= \frac{c}{4\pi}\mathrm{Re}[\mathbf{E}(\mathbf{r})\times\mathbf{B}(\mathbf{r})]_z \\ &= \frac{c\hbar}{16\pi|k_z|^2}\coth\left(\frac{\hbar\omega}{2k_BT}\right)\int\int\frac{d^2q}{(2\pi)^2}\frac{(k_z+k_z^*)(w_s+w_p)}{k}\frac{d^2q}{(2\pi)^2} \\ &= \frac{c\hbar k}{4\pi^2}\coth\left(\frac{\hbar\omega}{2k_BT}\right)\int_0^{\frac{\omega}{c}}dqq\frac{1-|R_p|^2+1-|R_s|^2}{2} \end{aligned} \tag{4.22}$$

Only propagating waves ($q < \omega/c$) contribute to this expression. Using (4.22) in (4.21), we get

$$I(\omega) = \frac{c\hbar k}{2\pi^2}\frac{1}{e^{(\hbar\omega/k_BT)}-1}\int_0^{\frac{\omega}{c}}dqq\frac{1-|R_p|^2+1-|R_s|^2}{2} \tag{4.23}$$

Introducing $d\Omega$, the elementary solid angle, we have the relation $qdq/k^2 = d\Omega\cos\theta/2\pi$. The radiated intensity is then given by

$$I(\omega) = \frac{\hbar\omega^3}{2\pi^2c^2}\frac{1}{e^{(\hbar\omega/k_BT)}-1}\int_\Omega\frac{d\Omega\cos\theta}{2\pi}\frac{1-|R_p|^2+1-|R_s|^2}{2} \tag{4.24}$$

where the integration is over the upper semi-sphere for $0 < \theta < \pi/2$. In the case of a black body, i.e. a body for which the reflection factors vanish, we get

$$I(\omega) = \frac{\hbar\omega^3}{4\pi^2c^2}\frac{1}{e^{(\hbar\omega/k_BT)}-1} = \pi I_0(\omega,T) \tag{4.25}$$

where

$$I_0(\omega,T) = \frac{\hbar\omega^3}{4\pi^3c^2}\frac{1}{e^{(\hbar\omega/k_BT)}-1} \tag{4.26}$$

is the black body specific intensity. When the medium situated below the interface does not behave as a black body, the flux takes the classical form

$$I(\omega) = I_0(\omega,T)\int_\Omega\varepsilon'(\theta,\omega)\cos\theta d\Omega \tag{4.27}$$

where we have identified the emissivity $\varepsilon'(\theta,\omega) = (1-|R_p|^2+1-|R_s|^2)/2$. In the presence of a single interface, we note that the radiation emitted is not different from the usual one, i.e. near field does not play any role in this situation.

4.2 The Green's Function Approach

According to (A.4) outside of any body, the spectral correlation function for electric field is given by:

$$\left\langle E_i(\mathbf{r})E_j^*(\mathbf{r}')\right\rangle_\omega = \frac{\hbar c^2}{16\pi^2 i\omega^2}\coth\left(\frac{\hbar\omega}{2k_BT}\right) \times \int d\mathbf{S}_1''\Big\{D_{ik}(\mathbf{r},\mathbf{r}'')\nabla''D_{jk}^*(\mathbf{r}',\mathbf{r}'') - D_{jk}^*(\mathbf{r}',\mathbf{r}'')\nabla''D_{ik}(\mathbf{r},\mathbf{r}'')\Big\}. \tag{4.28}$$

For the plane surface, it is convenient to decompose the electromagnetic field into s- and p-polarized plane waves. The decomposition of the electromagnetic field on s- and p-polarized waves is determined by the vectors $\hat{n}_s = [\hat{z}\times\hat{q}] = (-q_y, q_x, 0)/q$, $\hat{n}_p^{\pm} = [\hat{k}^{\pm}\times\hat{n}_s] = (\mp q_x k_z, \mp q_y k_z, q^2)/(kq)$ where $\mathbf{k}^{\pm} = \mathbf{q} \pm \hat{z}k_z$, $k_z = ((\omega/c)^2 - q^2)^{1/2}$, $k = \omega/c$, $\mathbf{q}$ is the surface component of the wave vector. In this representation, the Green's tensor is given by

$$\hat{\mathbf{D}}(\mathbf{r},\mathbf{r}') = \int \frac{d^2q}{(2\pi)^2}\hat{\mathbf{D}}(z,z',\mathbf{q})e^{i\mathbf{q}\cdot(\mathbf{x}-\mathbf{x}')}, \tag{4.29}$$

and the spectral correlation function for the electric field is given by

$$\left\langle \mathbf{E}(\mathbf{r})\mathbf{E}^*(\mathbf{r}')\right\rangle_\omega = \frac{\hbar c^2}{16\pi^2 i\omega^2}\coth\left(\frac{\hbar\omega}{2k_BT}\right)\int\frac{d^2q}{(2\pi)^2} \times \Big(\hat{\mathbf{D}}(z,z'',\mathbf{q})\frac{\partial}{\partial z''}\hat{\mathbf{D}}^+(z',z'',\mathbf{q}) - \frac{\partial}{\partial z''}\hat{\mathbf{D}}(z,z'',\mathbf{q})\hat{\mathbf{D}}^+(z',z'',\mathbf{q})\Big)_{z''=+0} e^{i\mathbf{q}\cdot(\mathbf{x}-\mathbf{x}')}. \tag{4.30}$$

The Green's functions in (4.30) can be obtained from the Green's functions calculated in Appendix C in the vacuum gap between two semi-infinite plates, assuming the reflection amplitude for body two vanishes, $R_{2p(s)} = 0$. As a result we get the following expression for the Green's function in (4.30)

$$\hat{\mathbf{D}}(z,z') = \frac{2\pi i k^2}{k_z}\Big\{e^{\mathrm{i}k_z|z-z'|}\hat{\mathbf{I}} + \hat{\mathbf{R}}e^{\mathrm{i}k_z(z+z')}\Big\}, \tag{4.31}$$

where the 3×3 reflection matrix is given by

$$\hat{\mathbf{R}} = \hat{\mathbf{n}}^+ R\hat{\mathbf{n}}^-,$$

$\hat{\mathbf{n}}^{\pm} = (\hat{n}_s^{\pm}, \hat{n}_p^{\pm})$. The 2×2 reflection matrix $R_{\lambda\lambda'}$ determines the reflection amplitudes for the waves with different polarization $\lambda = (s, p)$. This matrix is diagonal for

isotropic materials. However, in the general case of anisotropic materials, this matrix is not diagonal

$$R = \begin{pmatrix} R_{ss} & R_{sp} \\ R_{ps} & R_{ss} \end{pmatrix}.$$

$\hat{\mathbf{I}}$ is the 3×3 unit matrix. The substitution of (4.31) in (4.30) gives

$$\left\langle \mathbf{E}(\mathbf{r})\mathbf{E}^*(\mathbf{r}') \right\rangle_\omega = \coth\left(\frac{\hbar\omega}{2k_B T}\right) \int \frac{d^2q}{(2\pi)^2} \left(\frac{\omega}{c}\right)^2 \hat{\mathbf{n}}^+ w \hat{\mathbf{n}}^{+*}, \tag{4.32}$$

where

$$w = \frac{\hbar}{4|k_z|^2}\left[(k_z + k_z^*)(I - RR^*) + (k_z^* - k_z)(R - R^+)\right],$$

where I is the 2×2 unit matrix. For the isotropic materials, the matrix w becomes diagonal: $w_{\lambda\lambda'} = w_\lambda \delta_{\lambda\lambda'}$ where

$$w_\lambda = \frac{\hbar}{4|k_z|^2}\left[(k_z + k_z^*)(1 - |R_\lambda|^2) + (k_z^* - k_z)(R_\lambda - R_\lambda^*)\right],$$

where $\lambda = (s, p)$.

For the evanescent waves we can use (3.64). In this case, the calculations are simpler. Taking into account the fact that, for the evanescent waves, k_z is pure imaginary ($k_z = i|k_z|$), we get

$$\hat{\mathbf{D}}(\mathbf{r}, \mathbf{r}', \omega) = 2\pi k^2 \int \frac{d^2q}{(2\pi)^2} \frac{e^{i\mathbf{q}\cdot(\mathbf{x}-\mathbf{x}') - |k_z|(z+z')}}{|k_z|} \hat{\mathbf{n}}^+ \mathrm{Im} R \hat{\mathbf{n}}^{+*} \tag{4.33}$$

Substituting these equation in (3.64) gives the part of (4.32) corresponding to the evanescent waves.

4.3 Density of Emitted Electromagnetic Energy

The energy density of the fluctuation electromagnetic field, radiated into the vacuum by the medium, which occupies half-space $z < 0$, is, according to (3.54), given by

$$u(\omega, T, \mathbf{r})d\omega = \frac{1}{8\pi}\left[2\langle \mathbf{E}(\mathbf{r})^2 \rangle_\omega + 2\langle \mathbf{H}^2 \rangle_\omega\right] d\omega. \tag{4.34}$$

Using (4.34) with (4.3) and (4.19), the total electromagnetic energy, radiated by the solid at a temperature of T in the vacuum at a temperature of 0 K at a distance of z from the surface of medium, is given by

$$u(\omega, T, z) = \frac{\Pi(\omega, T)\omega^2}{4\pi^2 c^3}\left\{\int_0^{\frac{\omega}{c}} \frac{dqq}{k|k_z|}\left[(1-|R_p|^2)+(1-|R_s|^2)\right]+\right.$$

$$\left.+2\int_{\frac{\omega}{c}}^{\infty} \frac{dqq^3}{k^3|k_z|}\left[\mathrm{Im}R_p+\mathrm{Im}R_s\right]e^{-2|k_z|z}\right\}, \tag{4.35}$$

where $k = \omega/c$, $\Pi(\omega, T)$ is determined by Plank's formula

$$\Pi(\omega, T) = \frac{\hbar\omega}{e^{\beta\hbar\omega}-1}. \tag{4.36}$$

In (4.36), we do not take into account the temperature-independent contribution from the zero-point oscillations of the electromagnetic field.

Let us apply the general equation (4.35) for concrete materials. Let us first consider a material that supports surface waves in the infrared, such as silicon carbide (SiC). Figure 4.1 shows the energy density $u(\omega, T, z)$ versus the frequency at different distances from a semi-infinite solid of SiC. The semi-infinite medium is at temperature $T = 300$ K whereas the vacuum is at $T = 0$ K. Note that at $T = 300$ K, Wiens law gives a peak wavelength for thermal radiation of $\lambda_W = 10$ μm. In the

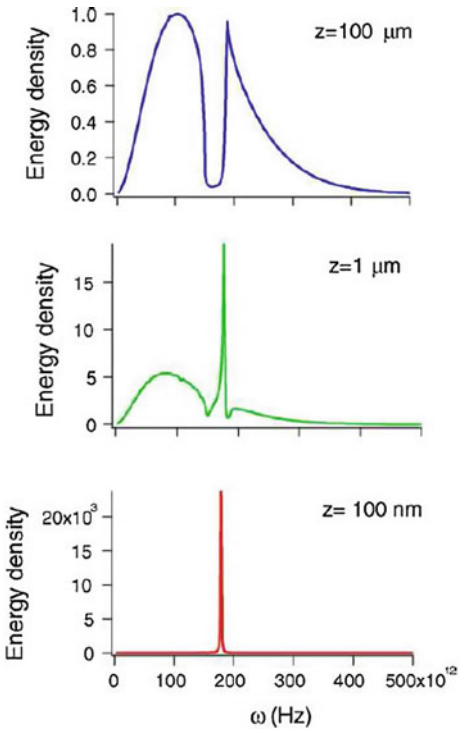

Fig. 4.1 Total electromagnetic energy density above a plane interface separating SiC at $T = 300$ K from vacuum at $T = 0$ K. From [9]

far field, i.e. for distances $z \gg \lambda_W$, the energy density spectrum resembles that of a black body. The difference from that of a Planck spectrum comes from the fact that SiC is a material with a high reflectivity of around $\lambda_W = 10\ \mu\text{m}$ or $\omega = 1.7 \times 10^{14}\ \text{s}^{-1}$. Thus, its emissivity is small at this frequency. This property follows from the expression for the electromagnetic energy due to propagating waves only (first term in (4.35))

$$u^{prop}(\omega, T, z) = u^0(\omega, T) \int \frac{d\Omega}{4\pi} \frac{\left[(1 - |R_p|^2) + (1 - |R_s|^2)\right]}{2}, \tag{4.37}$$

where we have used $2\pi q dq = k^2 \cos\theta d\Omega$, and where θ is the angle between the emission direction and the normal of the surface. The integral is performed over a half-space and $u^0(\omega, T) = (\omega^2/\pi^2 c^3)\Pi(\omega, T)$ is the electromagnetic energy density in a cavity at thermal equilibrium T. In the far field, the evanescent waves do not contribute to the energy density because of the exponential decay $e^{-2|k_z|z}$. We note that if the medium is totally absorbing ($R_{p(s)} = 0$), then the energy density due to propagating waves is half the energy calculated in a vacuum at thermal equilibrium. This is not surprising, since we are computing only the emitted part of the radiation. In the case of equilibrium radiation, there is also the contribution of the radiation coming from the upper half-space. At a distance $z = 1\ \mu\text{m}$, which is slightly larger than λ_W, the energy density spectrum changes drastically and a strong peak emerges. At $z = 100$ nm, one observes that the thermal emission is almost monochromatic around $\omega = 1.79 \times 10^{14}\ \text{s}^{-1}$. At this frequency, the energy density has increased by more than four orders of magnitude. The peak corresponds to the excitation of a surface wave. This distance is in agreement with the decay length of the surface waves as discussed in Chap. 2. At distances much smaller than the wavelength, we enter a regime that we denote as the extreme near field region. The leading contribution now comes from the very large wavevectors q in the energy density integral. At large q, it can be shown that $k_z \approx k_{z1} \approx iq$, so that R_s tends to $\approx (\varepsilon - 1)(\omega/2cq)^2$ and R_p tends to its electrostatic limit $(\varepsilon - 1)/(\varepsilon + 1)$. In this case, the contributions to the density of the electric energy from p- and s-polarized electromagnetic waves are given by

$$u_p(\mathbf{r}, \omega) = \frac{1}{8} u^0(\omega, T) \left(\frac{c}{\omega d}\right)^3 \frac{\varepsilon''}{|\varepsilon + 1|^2}, \tag{4.38}$$

$$u_s(\mathbf{r}, \omega) = \frac{1}{16} u^0(\omega, T) \left(\frac{c}{\omega d}\right) \varepsilon'', \tag{4.39}$$

where ε' and ε'' are the real and imaginary part of dielectric function $\varepsilon = \varepsilon' + i\varepsilon''$, and $u^0(\omega, T)$ is the density of the electromagnetic energy for *black body radiation*. For p-polarized electromagnetic waves and $\varepsilon'' \ll 1$, the near-field emission spectrum has a strong peak near the frequency ω_0 defined by the condition $\varepsilon'(\omega_0) = -1$. This effect results from the existence of a large number of surface modes with different wave numbers but with frequencies $\omega \approx \omega_0$ that are very close to each other. Therefore, if ε'' is not very large at $\omega = \omega_0$ the density of surface modes will necessarily

display a strong peak at $\omega = \omega_0$. From (4.38) and (4.39), it follows that $u_s/u_p \sim |\varepsilon + 1|^2(\omega d/c)^2$. For metals, $|\varepsilon| \gg 1$, and therefore the contribution in energy density from the s- polarized waves for the infrared frequencies will exceed contribution from the p- polarized waves up to the very small distances. The presence of surface waves is the origin of the peak in the near-field spectrum of SiC at $\omega = 1.78 \times 10^{14}$ s^{-1}. However, since the surface waves decay exponentially away from the surface, this peak will vanish in the far zone. The presence of a resonance in the density of modes $N(z, \omega)$ is, however, not required for observing spectral changes caused by the loss of evanescent modes. Indeed, in the short-distance regime, the spectrum is given by (4.38), whereas, in the far-field, the spectrum is given by (4.37). Thus, even in the absence of resonant surface waves, the near-field spectrum is different from the far-field spectrum, but the changes are less dramatic.

Not all materials that support surface waves exhibit strong peaks in their near-field thermal energy density spectrum. Indeed, as can be seen in (4.38), a peak is exhibited if the frequency where $\varepsilon(\omega)$ approaches -1 corresponds to a frequency range where $\Pi(\omega, T)$ is not too small. For example, metals exhibit surface plasmon polariton in the UV or visible range where $\Pi(\omega, T)$ is exponentially small at ambient temperature. Thus, metals do not exhibit any strong peak in their thermal energy density spectrum in the near field.

4.4 Local Density of States

The density of states (DOS) is a fundamental quantity from which many macroscopic quantities can be derived. In statistical physics, the DOS allows the partition function of a system, from which all the macroscopic properties follow, to be calculated. The local density of states (LDOS) is useful for studying a non-uniform system. The local density of electronic states is widely used in solid-state physics. It has been shown [192], for instance, that a scanning tunneling microscope images the electronic LDOS. The local character of the LDOS clearly describes the spatial distribution of electrons in the solid. A similar spatial dependence is also relevant for electromagnetic waves. Whereas the intensity is uniform in vacuum in equilibrium, this is not the case in a waveguide or above an interface. In addition, while the LDOS is well known and frequently used for electrons in solid-state physics [37], its electromagnetic counterpart is not well known or used in the literature. Compared with electronic systems, two differences must be taken into account: the vectorial nature of the fields and the existence of losses.

We consider a system in thermal equilibrium at temperature T. In a vacuum, one can define the electromagnetic energy $U(\omega)$ by the product of the DOS $\rho(\omega)$ and the mean energy of each state at temperature T:

$$U(\omega) = \rho(\omega)\frac{\hbar\omega}{\exp(\hbar\omega/k_B T) - 1}. \tag{4.40}$$

We now introduce an LDOS by using, as a starting point, the local density of electromagnetic energy $u(\mathbf{r}, \omega)$ at a given point $\mathbf{r}$ in space, and at a given angular frequency ω. We define the LDOS $\rho(\mathbf{r}, \omega)$ so that

$$u(\mathbf{r}, \omega) = \rho(\mathbf{r}, \omega) \frac{\hbar\omega}{\exp(\hbar\omega/k_B T) - 1}. \tag{4.41}$$

Using (4.35) for the LDOS for p- and s-propagating electromagnetic waves, we get

$$\rho_{p(s)}^{propE} = \rho_{p(s)}^{propH} = \frac{\rho_v}{4} \int_0^{\frac{\omega}{c}} \frac{dqq}{kk_z} \left(1 - |R_{p(s)}|^2\right), \tag{4.42}$$

where the superscripts E and H denote the electric and magnetic contributions, respectively; $\rho_v(\omega) = \omega^2/\pi^2 c^3$ is the vacuum density of states, and for the contributions from the evanescent waves we get

$$\rho_{p(s)}^{evanE(H)} = \frac{\rho_v}{2} \int_{\frac{\omega}{c}}^{\infty} \frac{dqq}{k|k_z|} \left(\frac{2q^2}{k^2} - 1\right) \mathrm{Im} R_{p(s)} e^{-2|k_z|z}, \tag{4.43}$$

$$\rho_{s(p)}^{evanE(H)} = \frac{\rho_v}{2} \int_{\frac{\omega}{c}}^{\infty} \frac{dqq}{k|k_z|} \mathrm{Im} R_{s(p)} e^{-2|k_z|z}. \tag{4.44}$$

From (4.42)–(4.44), it follows that, for the propagating electromagnetic waves, the energy of the magnetic field is equal to the energy of the electric field. For the evanescent waves, taking into account that $\left(2q^2/k^2 - 1\right) > 1$, we get that, for p-polarized waves, the dominate contribution to the energy comes from the electric field, and, for s-polarized waves, the dominate contribution comes from the magnetic field. This difference is explained as follows: for the plane wave, the electric field is related to the induction magnetic field by $(c/\omega)[\mathbf{k} \times \mathbf{E}] = \mathbf{B}$, where $\mathbf{k} = \mathbf{q} + \hat{z}k_z$. Thus, for the s-polarized waves, we obtain the relationship $|\mathbf{k}|(c/\omega)|E| = |B|$. For the propagating waves, $|\mathbf{k}| = \sqrt{q^2 + k_z^2} = (\omega/c)$; therefore $|E| = |B|$, which means the equality of the magnetic and electric energy. For the evanescent waves of $k_z = i\sqrt{q^2 - (\omega/c)^2}$; therefore

$$|\mathbf{k}| = \sqrt{q^2 + k_z k_z^*} = \sqrt{2q^2 - \left(\frac{\omega}{c}\right)^2}.$$

Thus, $|B| = \sqrt{2(cq/\omega)^2 - 1}|E| > |E|$, which means that the magnetic energy is larger than electric energy. Similarly, it is possible to show that for the p-polarized evanescent waves, $|E| = \sqrt{2(cq/\omega)^2 - 1}|B| > |B|$, i.e., in this case the electric energy is larger than magnetic energy.

Using (4.42)–(4.44) and the Fresnel's formulas for the reflection amplitudes, we get that in the limit $z \ll c/(\omega|\varepsilon|^{1/2})$, the contribution from the evanescent waves considerably exceeds the contribution from the propagating waves. In this limit

$$\rho_p^E = \frac{\rho_v}{8k^3z^3}\frac{\varepsilon''}{|\varepsilon+1|^2}, \tag{4.45}$$

$$\rho_s^H = \frac{\rho_v}{16kz}\varepsilon'', \tag{4.46}$$

$$\rho_p^H = \frac{\rho_v}{4kz}\frac{\varepsilon''}{|\varepsilon+1|^2}, \tag{4.47}$$

$$\rho_s^E = \frac{\rho_v}{6\sqrt{2}}\sqrt{|\varepsilon|+\varepsilon'}, \tag{4.48}$$

where, in obtaining (4.48), we have used that

$$\int_0^\infty dq e^{-2qd}\mathrm{Im}\frac{q-s}{q+s} \approx \int_0^\infty dq \mathrm{Im}\frac{q-s}{q+s} =$$
$$= \mathrm{Im}\left\{ \mid s_0 \mid e^{i\phi}\int_0^\infty dt \frac{t-\sqrt{t^2-1}}{t+\sqrt{t^2-1}}\right\} =$$
$$= \frac{1}{2}\mathrm{Im}\left\{ \mid s_0 \mid e^{\mathrm{i}\phi}\int_{-\mathrm{i}\pi/2}^\infty \mathrm{d}z\left(e^{-z}-e^{-3z}\right)\right\} = \frac{2}{3} \mid s_0 \mid \cos(\phi),$$

where $s = \sqrt{q^2-(\omega/c)^2\varepsilon}$, $s_0 = (\omega/c)\sqrt{\varepsilon} = |s_0|\exp i\phi$. From comparison of (4.45)–(4.48) it follows that, for the metals in the infrared frequency region up to very small distances, the main contribution to the energy density comes from the magnetic field of the s-polarized electromagnetic waves.

4.5 Coherence Properties of Planar Thermal Sources in the Near-Field

Equations (4.3) and (4.19) describe the temporal and spatial coherence of the thermal radiation of the near field emitted into free space from the flat surface. Thermal radiation is often presented as a typical example of an incoherent light source and is in marked contrast to a laser. Whereas a laser is a highly monochromatic and very directional light source, a thermal source has a broad spectrum and is usually quasi-isotropic. However, as is often the case, different behavior can be expected on a microscopic scale. Thus, it has been shown [28–30] that the field emitted by a thermal source made of a polar material is enhanced by more than four orders of magnitude and is partially coherent at distances in the order of 10–100 nm. This phenomenon is due to surface electromagnetic waves, and can be observed only on material supporting them. The existence conditions for surface waves was considered in Chap. 2. Surface electromagnetic waves are modes that propagate along an interface, and decrease exponentially in the perpendicular direction (evanescent waves). The

propagation length of these surface waves is typically hundred wavelengths, resulting in a long-range spatial correlation of the electromagnetic field along the interface [28–30]. The near-field properties of the thermal electromagnetic field in the presence of surface electromagnetic waves were reviewed in [9].

There are different types of optically active surface waves. Surface phonon polaritons are observed for polar material such as SiC, glass, II–IV and III–V semiconductors. They are mechanical vibrations (phonons) propagating in a partially ionic material so that each unit cell becomes an oscillating electric dipole. Surface plasmon polaritons are longitudinal electron oscillations (acoustic type wave in an electron gas) that can be observed for metals and doped semiconductors, which generate electromagnetic fields with longitudinal polarization. Surface waves due to excitons, and vibrations of alkali ions in adlayers have also been observed.

Equations (4.3) and (4.19) also suggest a new application for near-field spectroscopy. The near-field spectrum at a given distance to the interface gives access to $\mathrm{Im}R_{p(s)}$, and one can hope to obtain information about the reflection amplitude for large wave vectors, similar to the method usually used to obtain $R_{p(s)}$ for propagating electromagnetic waves from reflectivity measurements. With the rapid development of near-field optical microscopy, such near-field spectra can be measured. This could open the way to a new technique of local solid-state spectroscopy. The measurement of thermal near-field using a scanning near-field microscope has been demonstrated recently [193]. This is an important step towards the concept of local spectroscopy.

4.5.1 Spatial Coherence in the Near-Field

The spatial coherence of the electromagnetic field is characterized by its spectral correlation function $\langle \mathbf{E}(\mathbf{r})\mathbf{E}(\mathbf{r}')\rangle_\omega$ at two different points for a particular frequency. Figure 4.2 represents the spectral correlation function of the electric field for different metallic surfaces at a given distance $z = 0.05\lambda$ ($\lambda = 2\pi c/\omega$ is the wavelength) to the interface. It can be seen that the correlation oscillates and has an exponentially decaying envelope. The decay length is much larger than the wavelength, indicating that the fields are coherent over large distances. This surprising phenomenon is due to the excitation of surface waves along the interface. The physical mechanism is based on the fact that a small volume element contains random currents that excite a surface wave. This surface wave propagates along the interface over distances larger than the wavelength. It follows that different points may be illuminated by the same random source so that they are correlated. Accordingly, one does not expect any correlation between the *s*-polarized field since no surface wave exists for *s*-polarization. If one uses a material with a real part of the dielectric constant larger than -1, no surface wave can propagate and thus no correlation should be observed. Therefore, Fig. 4.2 shows the case of tungsten in the visible that does not support surface waves. It is seen that the coherence length is smaller than a wavelength so that the radiation field appears to be more incoherent than blackbody radiation.

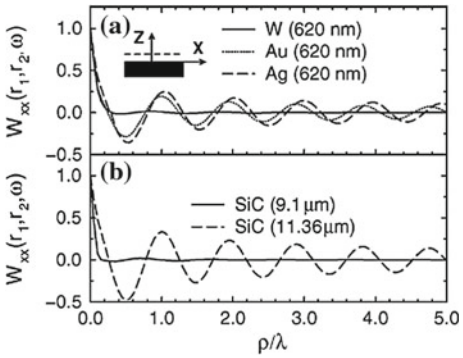

Fig. 4.2 Spectral correlation function $\langle E_x(\mathbf{r})E_x(\mathbf{r}')\rangle_\omega$ (denoted as W_{xx} in the label of the figure) of the thermally emitted x-component of the electric field vs. ρ/λ, where $\rho = |\mathbf{r}_1 - \mathbf{r}_2|$ **a** for different metals and **b** for SiC at different wavelengths. The long-range correlation is due to surface-plasmon polaritons for metals, and to surface-phonon polaritons for SiC. From [29]

A similar behavior is observed for SiC, a polar material that supports surface-phonon polaritons in a frequency band. Within this band, at a wavelength of 11.36 μm, a long-range correlation is observed, whereas for a wavelength (9.1 μm) that is not in the band where surface waves exist, the correlation decays very rapidly.

Let us discuss in simple terms the physical origin of these unusual coherence properties. The long-range coherence is unexpected because the fluctuating currents are δ-correlated as shown by the fluctuation-dissipation theorem. This is the reason why the fields are typically assumed to be δ-correlated in space. However, the fluctuating currents excite weakly damped collective modes in the material. In the case of a metal, a surface plasmon can be excited. In the case of a polar crystal, a surface phonon polariton can be excited. Both surface waves are extended modes along the surface. The induced currents associated with these extended modes are therefore coherent over large distances. More precisely, the coherence length is expected to be given by the decay length of these surface modes. This has been confirmed by a detailed asymptotic analysis in [31]. The other surprising property shown in Fig. 4.2 is that the coherence length defined as the FWMH of the cross-spectral density can be smaller than the wavelength. In other words, a source can be more spatially incoherent than the black body radiation. The key idea is that, close to an interface, the field contains evanescent waves so that features smaller than the wavelength can exist. This is not the case in a vacuum and therefore the field has a minimum coherence length. Since the amplitude of evanescent waves of large wavevector q decays as $\exp(-2qz)$, it is clear that the distance z appears as a cutoff wavelength. This explains the coherence length increasing as z increases into the near-field regime.

4.5.2 Temporal Coherence in the Near-Field

The temporal coherence of the electromagnetic field is characterized by the time-correlation function (at a fixed point $\mathbf{r}$ in space) of the electromagnetic field:

$$\left\langle E_k(\mathbf{r}, t+\tau) E_l(\mathbf{r}, t) \right\rangle \tag{4.49}$$

This correlation function is a measurement of the memory of the random field. It is useful to introduce a typical decay time t_{coh} of the correlation function, called coherence time. A Michelson interferometer with aligned mirrors performs a measurement of the correlation function. Indeed, the interference term of the signal can be written as $E_k(\mathbf{r}, t+\tau)E_l(\mathbf{r}, t)$ where τ is the flight time corresponding to the optical path length difference δ_{opt} between the two paths $\delta_{opt} = c\tau$. If the path length difference is larger than the longitudinal coherence length ct_{coh}, no interferences can be observed.

The temporal coherence of the EM field is related to its power spectral density. This is clearly seen by using the Wiener–Khinchin theorem [181, 182], which shows that the power spectral density is the Fourier transform of the correlation function. Alternatively, we can start from (3.24). It follows that:

$$\left\langle E_k(\mathbf{r}, t+\tau) E_l(\mathbf{r}, t) \right\rangle = \mathrm{Re}\left[\int_0^\infty 4\hbar n(\omega, T) \mathrm{Im}[D_{kl}^{EE}(\mathbf{r}, \mathbf{r}, \omega)] e^{i\omega\tau} \frac{d\omega}{2\pi} \right] \tag{4.50}$$

Let us first consider the temporal coherence of the field in vacuum. The imaginary part of the Green's tensor (3.46) does not diverge, and yields zero for non-diagonal terms and $\omega^3/3c^3$ for diagonal terms. It follows that the time-correlation function of the blackbody radiation is given by:

$$\left\langle E_k(\mathbf{r}, t+\tau) E_l(\mathbf{r}, t) \right\rangle = \delta_{kl} \mathrm{Re}\left[\int_0^\infty 4\Pi(\omega, T) \frac{\omega^2}{3c^3} e^{i\omega\tau} \frac{d\omega}{2\pi} \right] \tag{4.51}$$

Since the integrand has a large spectral width, it appears that the coherence time is in the order of the peak radiation period.

If we now consider the case of an interface, we know that the spectrum can be very different in the near field. We have seen previously that the contribution of the surface wave dramatically modifies the density of electromagnetic energy. In particular, we have seen that the density of energy becomes quasi-monochromatic, which suggests a large coherence time. More specifically, in the extreme near field, we have seen in Sect. 4.4 that the Green's function has a resonant denominator $\varepsilon + 1$. Close to the resonance where $\mathrm{Re}[\varepsilon(\omega_0)] = -1$, we can expand the dielectric constant as

$$\varepsilon(\omega) = -1 + i\varepsilon''(\omega_0) + (\omega - \omega_0)\frac{d\varepsilon'}{d\omega} \tag{4.52}$$

where we have used the notation $\varepsilon = \varepsilon' + i\varepsilon''$. Thus, the denominator $\varepsilon + 1$ can be cast in the form

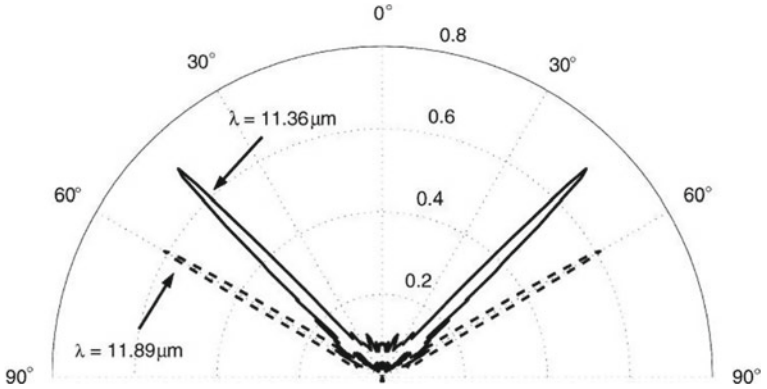

Fig. 4.3 Experimental angular emission of a SiC grating at two different wavelengths. The angular pattern has the characteristic shape of an antenna. It demonstrates the spatial coherence of the thermal source. Measurements are taken at 800 K. From [36]

$$\varepsilon(\omega) + 1 = \frac{d\varepsilon'}{d\omega}(\omega - \omega_0 + i\Gamma), \tag{4.53}$$

where $\Gamma = \varepsilon''/(d\varepsilon'/d\omega)$. It is seen that the Green's dyadic has a pole at the frequency corresponding to the asymptote of the dispersion relation of the surface wave. Its contribution to the integral (4.51) yields an exponential decay in the form $\exp(i\omega_0 t - \Gamma t)$. It follows that in the extreme near field, the thermally emitted field is temporally coherent with a coherence time given by Γ^{-1}. The origin of the temporal coherence of the electromagnetic field can thus be assigned to the very large density of states due to the surface wave. It follows that, whereas the plane interface of a hot metallic surface is a temporally incoherent source for an atom located in the far field, it is a partially temporally coherent source for an atom located within a nanometric distance from the interface.

4.5.3 Design of Coherent Thermal Sources

A spatially coherent source is a source that radiates a field that has a narrow angular aperture at a given wavelength. The typical examples of coherent sources are lasers and antennas. These sources have well-defined emission angular lobes. A narrow angular emission lobe is a signature of the spatial coherence of the field in the plane of the source. We have seen in the previous section that a source that supports a surface wave is partially spatially coherent along the surface. However, because these waves cannot propagate in vacuum, the coherence remains confined to the vicinity of the surface. However, it is possible to couple the surface waves to the propagating waves. This can be done in several ways. A practical way is to rule a grating on the surface. The grating can then diffract the surface wave. By properly choosing

the period of the grating, it is possible to control the angle of propagation of the diffracted light. This was first observed in [32–34] for a very deep grating ruled on a doped silicon surface. Such a material supports surface plasmon polaritons in the infrared. A more effective source was realized using a gold grating by Kreiter et al. [35]. In [38], a thermally stimulated midinfrared source was developed that emits radiation within a narrow range of wavelengths ($\delta\lambda/\lambda \leq 0.2$). In this experiment, the silicon wafer was covered by a metal film. A lattice of holes in the metal mediated the coupling of the surface plasmon states to the emitted light. This technology will afford tunable infrared emitters with high power in a narrow spectral band critical for sensing, spectroscopy and thermophotovoltaic applications. Figure 4.3 shows the angular emission pattern of a SiC grating. It can be clearly seen that the angular aperture is very narrow, indicating a large coherence length [36].